Dry-Deposited Single-Walled Carbon Nanotube Films Doped with MoO_x as Electron-Blocking Transparent Electrodes for Flexible Organic Solar Cells

Il Jeon[1], Kehang Cui[2], Takaaki Chiba[2], Anton Anisimov[3], Albert G. Nasibulin[4,5], Esko I. Kauppinen[4], Shigeo Maruyama[2]*, and Yutaka Matsuo[1]*

1: Department of Chemistry, School of Science, The University of Tokyo, 7-3-1 Hongo, Bunkyo-ku, Tokyo 113-0033, Japan

2: Department of Mechanical Engineering, School of Engineering, The University of Tokyo, 7-3-1 Hongo, Bunkyo-ku, Tokyo 113-8656, Japan

3: Canatu Ltd., Konalankuja 5, FI-00390 Helsinki, Finland

4: Department of Applied Physics, Aalto University School of Science, 15100, FI-00076 Aalto, Finland

5: Skolkovo Institute of Science and Technology, 100 Novaya str., Skolkovo, Moscow Region, 143025, Russia

Carbon nanotubes (CNTs) and graphene have emerged as materials for next-generation electrodes in organic solar cells (OSCs), offering a possible alternative to indium tin oxide (ITO)-based OSCs.[1] CNTs and graphene have excellent mechanical flexibility and are composed entirely of highly abundant carbon. Single-walled CNTs (SWCNTs) have advantages in terms of stretchability[2], ease of synthesis, and suitability for direct roll-to-roll deposition onto substrates, which translate into lower costs. SWCNTs and their application as transparent conductive films in photovoltaics have been the subject of active research[3-13]. Here we report the most effective structure to date for an ITO-free OSC and its application in flexible devices. High-quality direct- and dry-deposited SWCNT film doped with MoO_x function was fabricated and functioned as an electron-blocking (hole-transporting) transparent electrode. The

electrode's performance was further enhanced by applying an overcoat of poly(3,4-ethylenedioxythiophene)-polystyrenesulfonic (PEDOT:PSS). Flexible OSCs were fabricated using thieno[3,4-b]thiophene/benzodithiophene (PTB7), which is a high-performance photoactive material that requires no annealing. Our SWCNT OSC produced the highest power conversion efficiency (PCE) for an ITO-free OSC: 6.04%. This value is 83% that of the leading ITO-based OSC (7.48%). We anticipate that the methodology presented here will have applications beyond OSCs, extending to other photovoltaic applications such as recently developed perovskite solar cells. Our findings will help pave the way toward carbon-based flexible solar cells that can be produced by facile and stable processes.

Since C. W. Tang demonstrated a prototype in 1986,[14] OSCs have attracted a great deal of attention as solution-processable, flexible light-harvesting devices that have the potential to help meet the world's energy needs. The efficiency of OSCs has increased tremendously with the development of bulk heterojunctions in which conductive polymers are mixed with fullerene-based [6,6]-phenyl C_{61}-butyric acid methyl ester (PCBM)[15] to maximize exciton dissociation. The recent development of low band gap polymers has enabled absorption of longer, previously underutilized wavelengths of the solar spectrum and thus led to larger open-circuit voltage (V_{OC}) and short-circuit current (J_{SC}). As a result, PCEs have reached as high as 10%, which is currently the highest value among non-tandem OSCs. However, OSC flexibility[16] is still limited by the use of ITO, which can be made bendable but not completely flexible or stretchable like CNTs.

The objectives of this study are threefold. First, a free-standing CNT film was prepared by direct- and dry-deposition of SWCNTs grown by an aerosol chemical vapor deposition technique[17]. The performance of this film as a transparent conductor was the higher than that of other CNT films and flexible ITO. Compared with the preparation of SWCNT thin films by solution-based processes[18-20], our direct- and dry-deposition process uses less resources and induces no shortening or defects. Second, we discovered that MoO_x thermally annealed with SWCNTs exhibited dual functionality as both a strong p-dopant and

electron-blocking layer while exhibiting excellent stability. Thermally annealed MoO_3 doping, which was originally proposed by Bao *et al*.[21], was optimized and found to be the most effective methodology for fabricating the OSCs because other reported dopants were unstable to air, chemicals, thermal stress, and humidity. Third, three kinds of OSCs were made: a poly(3-hexylthiophene) (P3HT) system on glass, a PTB7 system on glass, and a PTB7 system on a flexible substrate. Most CNT OSCs reported to date use a P3HT system[3]. Therefore, valid comparisons were made through P3HT:PCBM devices. PTB7 has high performance and does not require thermal annealing[22]. As this enables the use of plastic substrates[23], we fabricated OSCs using the PTB7 system on both glass and flexible substrates. These OSCs produced PCEs of 2.43% for the P3HT:PCBM device and 6.04% for the PTB7:PCBM device. In addition, flexible OSCs on polyimide (PI) film and polyethylene terephthalate (PET) film gave PCEs of 3.43% and 3.91%, respectively.

We first investigated the thickness dependence of surface structures and basic electronic properties in the SWCNT films. By varying the deposition time, we produced SWCNT films with three thicknesses that gave 65%, 80%, and 90% transparency at 550 nm[24,25]. The atomic force microscopy (AFM) showed that all the SWCNT films had similar root mean square roughness of 8 to 10 nm (Fig. S2). Using P3HT:PCBM as the photoactive materials, OSCs were fabricated on ITO and SWCNT films with different thicknesses. MoO_3 was used here as an electron-blocking layer and it was not subjected to thermal annealing. The devices based on the SWCNT films of different thickness showed similar PCEs of under 1% (Table S1). These results were similar due to the trade-off between J_{SC} and fill factor (FF), which are related to transparency and conductivity, respectively. The poor performance was due to high series resistance (R_S) and low J_{SC}.

Then, the SWCNT films were thermally doped with MoO_3 and characterized. In previous work, MoO_3 under spray-coated SWCNTs was thermally annealed at 450–500 °C for more than 3 h in Ar and this enhanced the conductivity of the SWCNTs by activating charge transfer from CNT to MoO_3[21]. For use with the flexible PI substrate, which has a glass transition temperature (T_g) of 320 °C, we annealed the SWCNT film with MoO_3 on top at

300 °C for 3 h in N_2. MoO_3 changed from transparent green to deep blue after the annealing (Fig. S3). This was caused by the oxygen content being reduced from MoO_3 to MoO_x, where x is less than 3. UV–vis spectra showed that the SWCNT film annealed with MoO3 had higher transmittance at longer wavelengths compared with the pristine SWCNT film (Fig. S4a). Furthermore, the effect of MoO_x absorption was stronger in thinner SWCNT films (Fig. S4b). From this trend, we hypothesized that P3HT, which absorbs short wavelengths, would give higher PCE in the 90% transparent SWCNT electrode and that PTB7, which absorbs long wavelengths, would give higher PCE in the 65% transparent SWCNT electrode. Even without thermal doping, MoO_3 on a quartz substrate was found to have a small but notable effect where the absorption spectrum was extended toward the near-IR region (Fig. S5). This indicates that even without annealing, MoO_3 doping has an effect at the point of contact with the SWCNT film. The effect of doping was considerably enhanced after 2 h of thermal annealing (Fig. S5). A decrease in the resistance of the SWCNT films was found by four-probe measurement, providing further evidence of the effects of doping (Table S2).

The valence bands and work functions were measured by photoelectron yield spectroscopy in air and Kelvin probe force microscopy. We found that the thermal doping narrowed the gap between the Fermi levels of SWCNT and MoO_3 (Figure 1c). Pristine SWCNT films on glass exhibited a work function of 4.86 eV and a valence band of 5.12 eV. After thermal annealing, the work function increased to just above 5.4 eV. The work function of MoO_3 is reported to be 6.75 eV[26] and annealing MoO_3 decreased its work function to 6.00 eV.

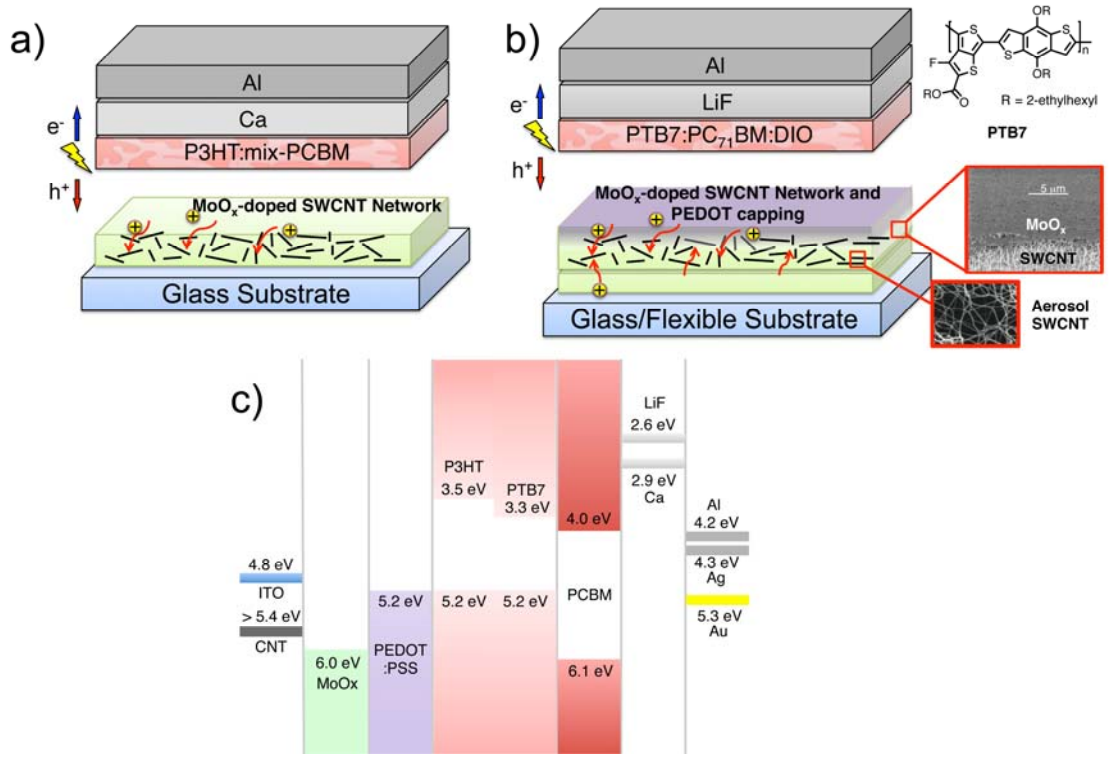

Figure 1. a) CNT OSC configuration with the P3HT system used for the structural investigations: glass/SWCNT/MoO_x/P3HT:mix-PCBM/Ca/Al. b) The optimized structure: glass or flexible substrate/MoO_x/SWCNT/MoO_x/PEDOT:PSS/PTB7:$PC_{71}BM$:DIO/LiF/Al. c) Energy band alignment diagrams of P3HT- and PTB7-based SWCNT OSCs. Red arrows denote thermally driven hole doping from MoO_3 to SWCNT to generate electron-blocking transparent electrodes.

When OSCs with P3HT and mix-PCBM[27] were fabricated using SWCNT films thermally annealed with MoO_3 (Fig. 1a), PCE was substantially improved to 1.47%, from 0.92% in the non-annealed MoO_3-based device (Table S3, devices A and B). Corresponding *J*–*V* curves are shown in Figure S6. We found that this improvement was due to both increased J_{SC} and decreased R_S. They were clear indications of improved transmittance and conductivity in the SWCNT films. A rather high shunt resistance (R_{SH}) was observed after thermal annealing (device B), indicating that the annealed MoO_x still functioned as an electron-blocking layer. However, low FF still posed an obstacle to good photovoltaic performance. Scanning electron microscopy and AFM images revealed that thermal annealing

increased the surface roughness (Fig. S7). Such unfavorable morphology can reduce FF. To find a solution to this, we tested various configurations involving additional non-annealed MoO_3 or PEDOT:PSS that could function as an electron-blocking layer and fill in the rough surface. Extra MoO_3 increased FF but decreased J_{SC} (Table S3, devices C and D), which may be attributable to mismatched band energy levels, whereas PEDOT:PSS with Li/Al improved performance greatly (Table S3). LiF/Al was found to be a more suitable cathode than Ca/Al (Table S4). With the optimized configuration of SWCNT/MoO_x/PEDOT:PSS and LiF/Al, PCE of 2.34% was achieved (Table S3, device J). Moreover, the efficiency was enhanced by using a sandwich annealing structure, MoO_x/SWCNT/MoO_x/PEDOT:PSS, giving PCE of 2.43% (Table S3, device K), which is 86% that of the corresponding ITO/MoO_3-based OSC (2.83%; Table S1, Fig. 2a).

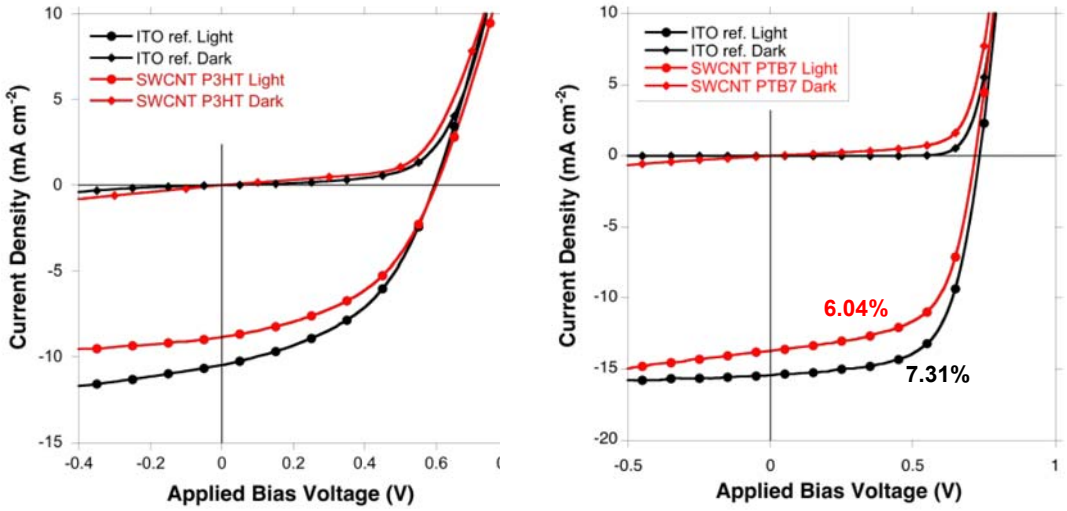

Figure 2. a) *J-V* curves of the two optimized CNT OSCs using the P3HT system under light and dark conditions. b) Light and dark *J-V* curves of optimized CNT OSCs using the PTB7 system.

Next, we switched the photoactive material to PTB7[22]. This low band gap polymer has a stabilized quinoidal structure, a rigid backbone, side chains on the ester and benzodithiophene moieties, and fluorine functionality. Consequently, PTB7 shows high performance, though it has yet not been used in CNT OSCs. The OSC based on the 65%

transparent SWCNT film gave a PCE of 6.04%, which is a record-high (Fig. 1b; see also Fig. 2b, Table 1). This result shows that the low band gap polymer system is compatible with existing SWCNT-based electrodes.

Finally, application in flexible devices was accomplished using both PI and PET as substrates. PI's high T_g of about 320 °C enabled thermal annealing of MoO_3 on SWCNT film. In contrast, PET has a relatively low T_g of about 80 °C and therefore could not be annealed. Initially, the flexible OSCs gave PCEs of 3.78% (PI) and 3.91% (PET) (Table 1, Fig. 3). We ascribe the decrease in performance of both the flexible devices to stress and damage to MoO_x film during fabrication as a result of the decrease in R_S (Table 1 and Table S5). Additionally, in the PI device, its low J_{SC} was limited by the intrinsically low transparency of the film (Fig. S9). Nonetheless, the PET-based device in which thermal annealing was not applied gave higher PCE than the PI-based device because the acidic PEDOT:PSS functions as a weak dopant[28]. After subjecting the devices to 10 flexing cycles (radius of curvature: 5 mm), the PET-based flexible OSC retained its performance but the PI-based flexible OSC had significantly decreased performance (Fig. S10; see also Table S5). Shrinking of the film at high temperature is suspected to be the problem.

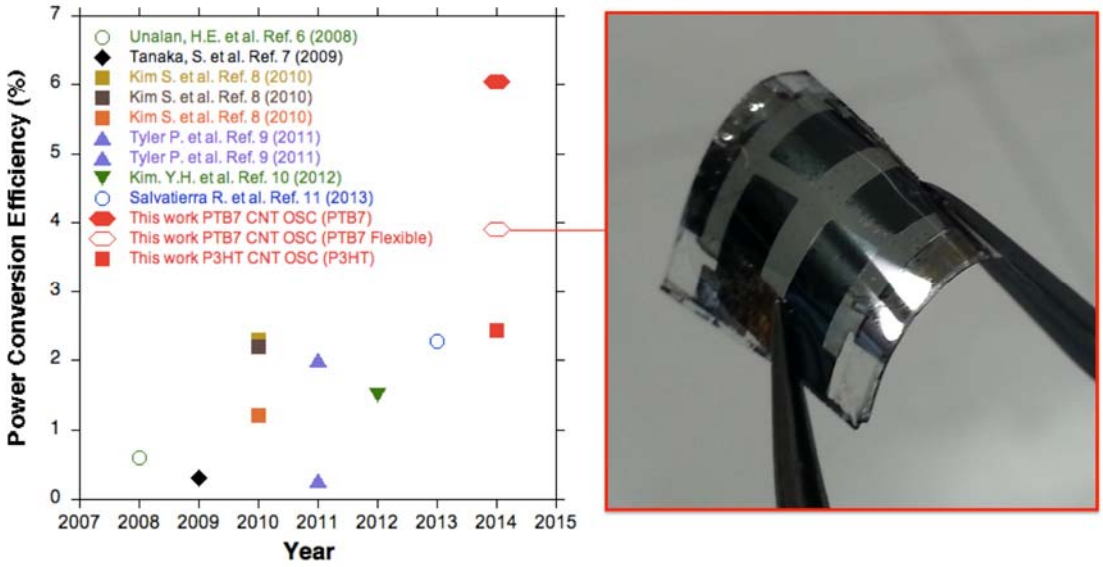

Figure 3. Reported record PCEs of CNT OSCs on glass (closed symbols) and on flexible substrate (open symbols) (left) and a picture of our PET-based flexible SWCNT OSC (right).

In summary, this work has shown the first application of direct- and dry-deposited SWCNT film in OSCs and demonstrated the dual functionality of thermally annealed MoO_x as both a dopant and electron-blocking layer. Thus, the SWCNT electrode doped with MoO_x by thermal annealing worked as an electron-blocking transparent electrode. Additional PEDOT:PSS coating was found to improve the surface roughness and electron-blocking ability. The PTB7 system produced record-high PCE for an SWCNT OSC on glass and was successfully used in a flexible device. Taken together, our findings demonstrate that ITO-free flexible SWCNT OSCs can be fabricated with high efficiency through a remarkably facile and stable process. We anticipate that these results will be useful in the further development of flexible carbon-based solar cells as well as other related organic electronics.

Table 1. Photovoltaic performance for the optimized SWCNT OSCs compared with the corresponding ITO-based references.

Device Configurations	V_{OC} (V)	J_{SC} (mA/cm^2)	FF	R_S (Ωcm^2)	R_{SH} (Ωcm^2)	PCE (%)
Glass/ITO/MoO_3/P3HT:mix-PCBM/Ca/Al	0.60	9.42	0.46	23.5	1.56E+04	2.83
Glass/*MoO_x/*SWCNT /*MoO_x/PEDOT:PSS/P3HT:mix-PCBM/LiF/Al	0.59	8.84	0.46	116	7.05E+03	2.43
Glass/ITO/MoO_3/PTB7:mix-PCBM/LiF/Al	0.74	15.5	0.64	31.1	1.18E+07	7.31
Glass/MoO_x/*SWCNT/*MoO_x/PEDOT:PSS/PTB7:PC_{71}BM/LiF/Al	0.72	13.7	0.61	51.6	1.22E+04	6.04
PI Film/MoO_x/*SWCNT/*MoO_x/PEDOT:PSS/PTB7:PC_{71}BM/LiF/Al	0.69	11.3	0.44	454	1.15E+05	3.43
PET Film/MoO_x/SWCNT/MoO_x/PEDOT:PSS/PTB7:PC_{71}BM/LiF/Al	0.69	12.6	0.45	160	2.06E+03	3.91

Note: *=Annealed at 300 °C for 3 hours under N_2 condition

References

[1] De Volder, M. F. L., Tawfick, S. H., Baughman, R. H. & Hart, A. J. Carbon nanotubes: present and future commercial applications. *Science* **339**, 535-539 (2013).

[2] Won, S. *et al*. Double-layer CVD graphene as stretchable transparent electrodes. *Nanoscale* **6**, 6057-6064 (2014).

[3] Du, J., Pei, S., Ma, L. & Cheng, H. Carbon nanotube- and graphene-based transparent conductive films for optoelectronic devices. *Adv. Mater.* **26**, 1958–1991 (2014).

[4] Park, H. *et al*. Flexible graphene electrode-based organic photovoltaics with record-high efficiency. *Nano Lett.* **14**, 5148–5154 (2014).

[5] Zhen, L. *et al*. Laminated carbon nanotube networks for metal electrode-free efficient perovskite solar cells. *ACS Nano* **8**, 6797-6804 (2014).

[6] Unalan, H. E. *et al.* Flexible organic photovoltaics from zinc oxide nanowires grown on transparent and conducting single walled carbon nanotube thin films. *J. Mater. Chem* **18**, 5909-5912 (2008).

[7] Tanaka, S. *et al.* Monolithic parallel tandem organic photovoltaic cell with transparent carbon nanotube interlayer. *Appl. Phys. Lett.* **94**, 113506- (2009).

[8] Kim, S. *et al*. Spin- and spray-deposited single-walled carbon-nanotube electrodes for organic solar cells. *Adv. Func. Mater.* **20**, 2310-2316 (2010).

[9] Tyler, T. P. *et al*. Electronically monodisperse single-walled carbon nanotube thin films as transparent conducting anodes in organic photovoltaic devices. *Adv. Energ. Mater.* **1**, 785 (2011).

[10] Kim, Y. H. *et al.* Semi-transparent small molecule organic solar cells with laminated free-standing carbon nanotube top electrodes. *Sol. Energy Mater. Sol. Cells* **96**, 244-250 (2012).

[11] Salvatierra, R. V., Cava, C. E., Roman, L. S. & Zarbin, A. J. G. ITO-free and flexible organic photovoltaic device based on high transparent and conductive polyaniline/carbon nanotube thin films. *Adv. Funct. Mater.* **23**, 1490-1499 (2013).

[12] Cui, K. *et al*. Air-Stable High-Efficiency Solar Cells Using Dry-Transferred Single-Walled Carbon Nanotube Films. *J. Mater. Chem. A* **2**, 11311-11318 (2014).

[13] Dabera, G. D. M. R. *et al*. Hybrid carbon nanotube networks as efficient hole extraction layers for organic photovoltaics. *ACS Nano* **7**, 556–565 (2013).

[14] Tang, C. W. 2-layer organic photovoltaic cell. *Appl. Phys. Lett.* **48**, 183–185 (1986).

[15] Yu, G. *et al*. Polymer photovoltaic cells: enhanced efficiencies via a network of internal donor-acceptor heterojunctions. *Science* **15**, 1789-1791 (1995).

[16]Kaltenbrunner, M. *et al*. Ultrathin and lightweight organic solar cells with high flexibility. *Nat. Commun.* **3**, 770 (2012).

[17] Nasibulin, A. G. *et al*. Multifunctional free-standing single-walled carbon nanotube films. *ACS Nano* **5**, 3214–3221 (2011).

[18] Zhou, Y., Hu, L. & Gruner, G. A method of printing carbon nanotube thin films. *Appl. Phys. Lett.* **88**, 123109 (2006).

[19] Lim, C., Min, D. H. & Lee, S. B. Direct patterning of carbon nanotube network devices by selective vacuum filtration. *Appl. Phys. Lett.* **91**, 243117 (2007).

[20] Wu, Z. *et al*. Transparent, conductive carbon nanotube films. *Science* **305**, 1273-1276 (2004).

[21] Hellstrom, S. L. *et al*. Strong and stable doping of carbon nanotubes and graphene by MoO_X for Transparent Electrodes. *Nano Lett.* **12**, 3574−3580 (2012).

[22] Liang, Y. *et al*. For the bright future—bulk heterojunction polymer solar cells with power conversion efficiency of 7.4%. *Adv. Mater.* **22**, E135–E138 (2010).

[23] He, Z. *et al*. Enhanced power-conversion efficiency in polymer solar cells using an inverted device structure. *Nat. Photonics* **6**, 591–595 (2012).

[24] Nasibulin, A. G. *et al*. Integration of single-walled carbon nanotubes into polymer films by thermo-compression, *Chem. Eng. J.* **136**, 409-413 (2008).

[25] Kaskela, A. *et al*. Aerosol synthesized SWCNT networks with tuneable conductivity and transparency by dry transfer technique. *Nano Lett.* **10**, 4349-4355 (2010).

[26] Irfan, *et al*. Energy level evolution of air and oxygen exposed molybdenum trioxide films. *Appl. Phys. Lett.* **96**, 243307 (2010).

[27] Santo, Y., Jeon, I., Yeo, K. S., Nakagawa, T. & Matsuo, Y. Mixture of [60] and [70] PCBM giving morphological stability in inverted organic solar cells, *Appl. Phys. Lett.* **103**, 073306 (2013).

[28] Kymakis, E. *et al*. Carbon nanotube/PEDOT:PSS electrodes for organic photovoltaics. *Eur. Phys. J. Appl. Phys.* **36**, 257-259 (2006).

Acknowledgements

This work was partly supported by the IRENA and MOPPI and Ministry of Education and Science of Russian Federation (Project DOI: RFMEFI58114X0006). The authors thank the Funding Program for Next-Generation World-Leading Researchers (Y.M.).

Author contributions

Y.M. and S.M. designed the project, with assistance in supervision from E.K. K.C. provided advice throughout the project and initially inspired doping method while I.J. conceived and carried out the experiments. Mainly, I.J. and Y.M. wrote the manuscript. I.J., K.C., and T.C. performed the measurements. A.G.N. and A.A. synthesized, and provided SWCNTs for the experiments.

Additional information

The authors declare no competing financial interests. Correspondence and requests for materials should be addressed to Yutaka Matsuo (matsuo@chem.s.u-tokyo.ac.jp) and Shigeo Maruyama (maruyama@photon.t.u-tokyo.ac.jp).

Supplementary Information

Dry-Deposited Single-Walled Carbon Nanotubes Doped with MoO_x as Electron-Blocking Transparent Electrodes for Flexible Organic Solar Cells

Il Jeon[1], Kehang Cui[2], Takaaki Chiba[2], Anton Anisimov[3], Albert G. Nasibulin[4,5], Esko I. Kauppinen[4], Shigeo Maruyama[2]*, and Yutaka Matsuo[1]*

1: Department of Chemistry, School of Science, The University of Tokyo, 7-3-1 Hongo, Bunkyo-ku, Tokyo 113-0033, Japan

2: Department of Mechanical Engineering, School of Engineering, The University of Tokyo, 7-3-1 Hongo, Bunkyo-ku, Tokyo 113-8656, Japan

3: Canatu Ltd., Konalankuja 5, FI-00390 Helsinki, Finland

4: Department of Applied Physics, Aalto University School of Science, 15100, FI-00076 Aalto, Finland

5: Skolkovo Institute of Science and Technology, 100 Novaya str., Skolkovo, Moscow Region, 143025, Russia

1. Experimental Procedures and Characterizations

1.1 Aerosol SWCNT preparation

SWCNTs were synthesized by an aerosol (floating catalyst) CVD method based on ferrocene vapor decomposition in a CO atmosphere[23]. The catalyst precursor was vaporized by passing ambient temperature CO through a cartridge filled with ferrocene powder. The flow containing ferrocene vapor was then introduced into the high-temperature zone of a ceramic tube reactor through a water-cooled probe and mixed with additional CO. To obtain stable growth of SWCNTs, a controlled amount of CO_2 was added together with the carbon source (CO). SWCNTs were directly collected downstream of the reactor by filtering the flow through a nitrocellulose or silver membrane filter (Millipore Corp., USA; HAWP, 0.45 μm pore diameter)[15,23].

1.2 Device fabrication

1.2.1 ITO-based OSC substrates

For the reference device, ITO substrates with size 15 × 15 mm^2 and an active area of 3 × 3 mm^2 with a sheet resistance of 6 Ω/square (Kuramoto Co., Ltd.) were sonicated in cleaning surfactant (Semi Clean, M-Lo), water, acetone and 2-isopropanol for 15 minutes each. The substrates were then dried in an oven at 70 °C. ITO substrates were exposed to UV/O_3 for 30 min in order to remove any remaining organic impurities.

1.2.2 SWCNT-based OSC substrates

For the SWCNT device, ITO substrates above were first etched using Zn and 1M HCl, followed by sonicating the substrates sequentially in cleaning surfactant (Semi Clean, M-Lo), water, acetone and 2-isopropanol for 15 minutes each. The substrates were then dried in an oven at 70 °C. Prior to SWCNT transfer, the bare glass substrates were exposed to UV/O_3 for 30 min. For the flexible device, Low Colour Polyimide film – 25 μm thickness from Industrial Summit Technology (IST) ltd. and Toyobo ltd. polyethylene terephthalate (A4300-38 μm) were used. The films were cleaned by ethanol and clean gauze.

1.2.3 SWCNT transfer to substrates

SWCNT films were transferred onto the substrates by laminating from the top so that it can have an active area between 3 × 4 to 3 × 2 mm^2 depending on samples. A drop of ethanol was used where there is no MoO_3 layer to ensure a firm adhesion of SWCNT. Use of ethanol dissolved MoO_3, although it was found to be not critical to the photovoltaic

performance. Then the substrates were transferred to a nitrogen filled glove box for further fabrication.

1.2.4 MoO_3 and PEDOT:PSS electron-blocking layer deposition on SWCNT

MoO_3, functioning as both an electron-blocking layer and dopant, was deposited under vacuum via a thermal evaporator. 15 nm MoO_3 was deposited with the average rate of 0.2 Å/s. In the case of SWCNT deposition, a poly-(3,4-ethylenedioxythiophene)-polystyrenesulfonic acid (PEDOT:PSS) dispersed in water (Clevios P VP, Heraeus Precious Metals GmbH & Co.) was spin-coated on top of the MoO_x to assist the electron-blocking ability by and filling up the pin holes formed from high temperature annealing.

1.2.5 PH3T:PCBM photoactive layer deposition on SWCNT

For the PH3T:PCBM photoactive layer deposition, a poly(3-hexylthiophene) (P3HT, regioregular, Sigma Aldrich Chemical Co., Inc.) and [6,6]-phenyl C61-butyric acid methyl ester and [6,6]-phenyl C71-butyric acid methyl ester in 16:3 ratio (mix-PCBM) (Frontier Carbon Co., Nanom spectra E124) solution with a donor:acceptor ratio of 5:3 and concentration of 40 mg/ml in ortho-dichlorobenzene (anhydrous, 99%, Sigma Aldrich Chemical Co., Inc.) was prepared[S1]. The solution was left stirring for 2 h at 65 ºC. The solution was then spin-coated on PEDOT:PSS layer at a speed of 2000 rpm for 90 s to give films of approximately 140 nm. The dried-up active layer did not require any solvent annealing. Instead, thermal annealing at 150 ºC for 14 minutes was performed.

1.2.6 PTB7:$PC_{71}BM$:DIO photoactive layer deposition on SWCNT

For the PTB7:$PC_{71}BM$:DIO photoactive layer deposition, thieno[3,4-b]thiophene/ benzodithiophene (PTB7) and [6,6]-phenyl C71-butyric acid methyl ester ($PC_{71}BM$) were purchased from Luminescence Technology Corporation and used as received without further purification. A blend solution of PTB7 and $PC_{71}BM$ was prepared in mixed solvents chlorobenzene (99%, CB) and 1,8-diiodoctane (DIO) at 97 : 3%. PTB7 (10 mg) and $PC_{71}BM$ (15 mg) were initially dissolved in CB inside a nitrogen glove-box (970 µl). The solution was left stirring overnight at 60 °C. After 24 h, the corresponding amount of DIO (30 µl) was added. The new solution was stirred 1 h at 70 °C. The solution of PTB7:$PC_{71}BM$:DIO (80 nm) was spin-coated at 1500 rpm for 60 s on PEDOT:PSS layer to give approximately 100 nm. No thermal annealing was required.

1.2.7 Cathode deposition on photoactive layer

For the cathodes, either Ca (10nm) or LiF (0.7nm) followed by Aluminium (100nm) was deposited by vacuum thermal evaporation. Other metals (100 nm) were also deposited in this way at the rate of 0.2 Å/s.

1.3 Characterizations

1.3.1 Photovoltaic characterization

Current-voltage (*J*-*V*) characteristics were measured by software-controlled source meter (Keithley 2400) in dark conditions and 1 sun AM 1.5G simulated sunlight irradiation (100 mW/cm^2) using a solar simulator (EMS-35AAA, Ushio Spax Inc.), which was calibrated using a silicon diode (BS-520BK, Bunkyokeiki). For the bending test of flexible devices, J−V measurements were recorded after 10 compressive flexing cycles (radius of curvature: 5 mm)

1.3.2 Other characterizations

Topography images were recorded using an AFM operating in tapping mode (SPI3800N, SII). SEM measurement was carried out on S-4800 (Hitachi). Valence band information and Fermi levels were measured by Riken Keiki PYS-A AC-2 and kelvin probe S spectroscopy in air (ESA), respectively. They were calibrated by Au before the measurement. Both homemade system based on Seki Technotron STR-250 (excitation wavelength 488nm) and inVia Raman microscope (Renishaw) were used for the Raman measurement. Shimadzu UV-3150 was used for the UV-vis-NIR measurement.

1.4 Experimental Pictures

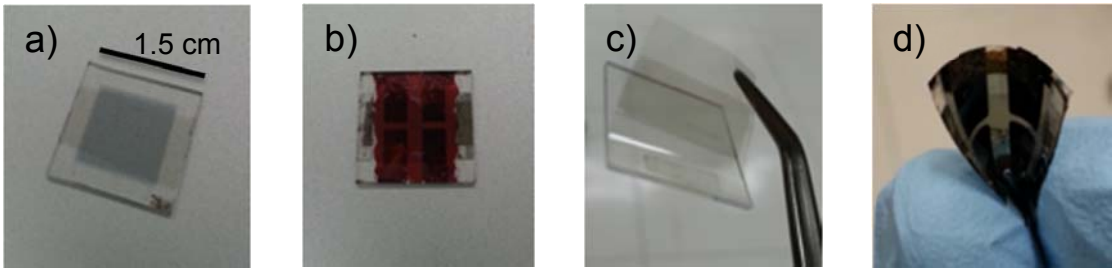

Figure S1. Pictures of a) MoO_3 doped SWCNT on a glass substrate. b) SWCNT OSC using a P3HT:PCBM system. c) SWCNT on a polyimide film supported by a glass substrate. d) Flexible SWCNT OSC using a PTB7:$PC_{71}BM$ system on a polyimide film.

2. SWCNT Thickness Comparison Before Thermally Doping MoO_3

2.1 Comparison of SWCNTs by AFM images and r.m.s. roughness values

SWCNT films with different thicknesses namely, 65%, 80%, and 90% according to their transparency at 550 nm wavelengths were produced. AFM analyses show that there are no significant differences in the r.m.s. among SWCNTs with different thicknesses. This dispenses the influence of morphology when studying SWCNTs with different thicknesses in OSC devices. Also During the MoO_3 deposition, achieving conformal coverage on the ridges in the SWCNTs was critical, since insufficiently covered SWCNT humps can serve as potential shunt pathways. Therefore, MoO_3 with 15 nm above was deposited.

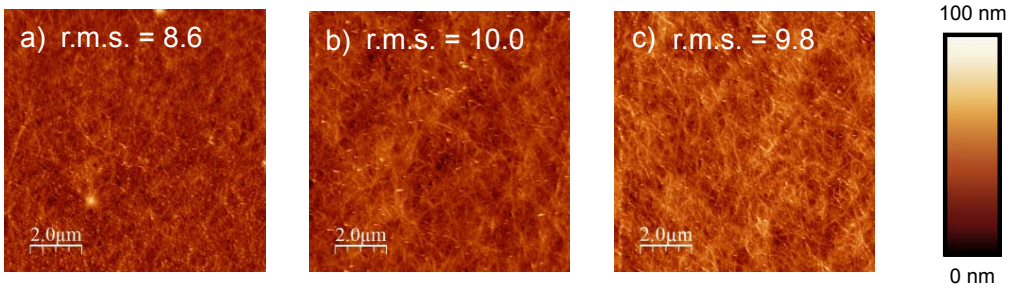

Figure S2. AFM images and r.m.s. roughness values of SWCNTs with different thicknesses a) 90% transparent SWCNT, b) 80% transparent SWCNT, c) 65% transparent SWCNT.

2.2 Comparison of SWCNTs with different transparency in P3HT:PCBM OSCs

For the investigation of the device structures, we fabricated OSCs using pristine SWCNTs without any doping in a configuration such that glass/SWCNT/MoO_x/P3HT:mix-PCBM/Ca/Al. Ca and Al were used as cathode because they have been reported to work the best with the P3HT:PCBM system[S2]. In this work, fast growth[S3] method of P3HT:PCBM was adopted for it does not consume a large quantity of materials and produce high enough performance without need for solvent annealing.

Table S1. Aerosol SWCNTs with different transparency have been fabricated to compare its influence on the overall efficiency as OSC electrode without doping effect.

Anode	Cathode	V_{OC} (V)	J_{SC} (mA/cm^2)	FF	R_S (Ωcm^2)	R_{SH} (Ωcm^2)	PCE (%)
ITO/MoO_3	Ca/Al	0.60	9.42	0.46	23.5	1.56E+04	2.83
SWCNT 90%/MoO_3	Ca/Al	0.59	4.74	0.33	1480	2.23E+03	0.92
SWCNT 80%/MoO_3	Ca/Al	0.54	4.54	0.39	201	7.66E+03	0.95
SWCNT 65%/MoO_3	Ca/Al	0.52	3.30	0.54	198	2.42E+04	0.93

3. Thermal Doping Effect of MoO_3

3.1 UV-Vis transmittance spectrum of an annealed MoO_x film

The color change of MoO_3 to deep blue after annealing in anaerobic condition verifies the presence of nonstoichiometric oxide. Such oxygen deficiency induces formation of electron traps and increases absorbance in the deep-blue wavelengths region[S4]. As this measurement was done on a glass substrate without CNT, the absorption is greater than the ones shown in Figure S4b, because with CNT, the change transfer from CNT to MoO_x should fill up the electron deficient traps. Incidentally, x value in MoO_x is supposed to be different when annealed on SWCNT.

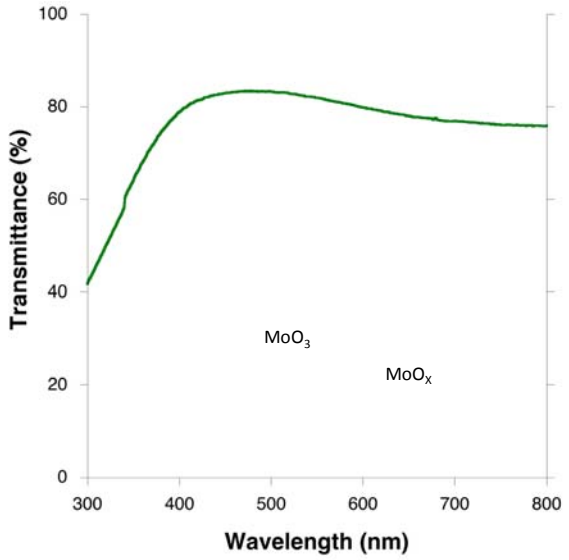

Figure S3. UV-Vis spectrum of an annealed MoO_x film on glass. Substrate spectrum has been subtracted from the MoO_x/glass substrate spectrum.

3.2 UV-Vis transmittance spectra of SWCNTs with different thicknesses before and after MoO_3 doping

UV-Vis spectroscopy on MoO_3 doped SWCNT shows the difference in transmittance among 65%, 80%, and 90% SWCNTs gets smaller after the thermal doping. This is because of the influence from MoO_x absorption. Thinner the SWCNT, the more it will manifest the shape of MoO_x transmittance spectrum. Therefore, while short-wavelengths absorbing P3HT may favor 90% transparent SWCNT electrode, long-wavelengths absorbing PTB7 can give higher PCE with 65% transparent SWCNT electrode.

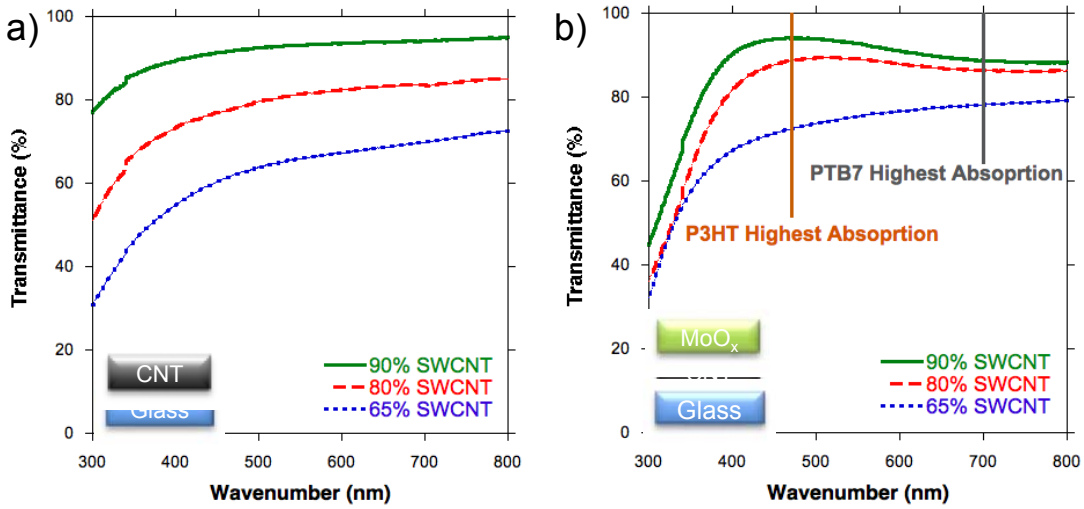

Figure S4. The UV-Vis data of SWCNTs with different thicknesses and indications of the highest absorption peak of P3HT and PTB7 a) for pristine SWCNTs b) for SWCNTs after depositing MoO_3 and thermally annealing at 300 °C for 3 h in N_2.

3.3 Vis-IR absorption spectra of thermally annealed MoO_3 on 90% SWCNTs

SWCNT's doping effect is confirmed by absorption spectra stretching along the near IR region on quartz substrates. Clear transitions of E_{11}, E_{22}, and M_{11} peaks indicate the high quality and small bundle size of aerosol CVD synthesized SWCNTs are suppressed a little when MoO_3 is deposited on SWCNT, and almost completely when MoO_3 deposition is followed by 2 h of thermal annealing.

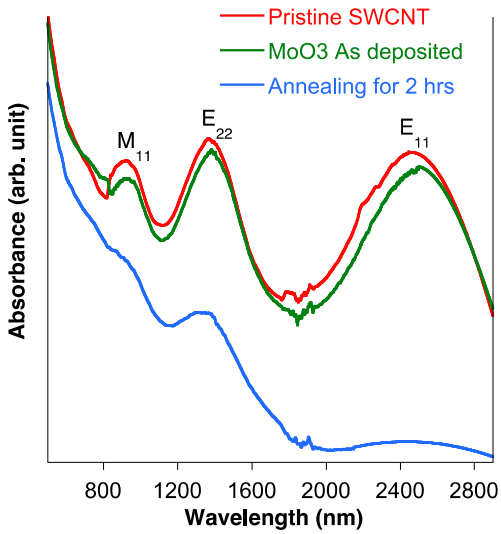

Figure S5. Absorption spectra of CNT pristine (red circles), CNT with MoO_3 on top (green squares), and CNT with MoO_3 on top after 2 h of annealing (purple filled squares).

3.4 Conductivity

Table S2. Four-probe measurement results of the pristine SWCNTs with different transparency and after MoO_3 thermal doping.

	Resistivity of 65% transparent SWCNT (Ω/sq.)	Resistivity of 80% transparent SWCNT (Ω/sq.)	Resistivity of 90% transparent SWCNT (Ω/sq.)
Pristine SWCNT	83.89	205.08	326.05
MoO_3 doped SWCNT	28.49	73.97	101.55

4. Optimization of the Device Structure

4.1 Various device configurations

4.1.1 Introduction of additional electron-blocking layers

Thermally annealed MoO_3 on 90% transparent SWCNT electrodes were used for the device structure investigation. Device performance improved significantly by thermally doping SWCNT with MoO_3 (Table S3, device A to B). However, low FF means that the device structure can be further optimized. Various combinations of annealed MoO_x, non-annealed MoO_3, and PEDOT:PSS in different arrangements were fabricated in order to improve the FF.

First of all, using non-annealed MoO_3, we devised two structures: one where annealed MoO_x sits beneath SWCNT (device C) and another where annealed MoO_x sits above SWCNT (device D), then depositing a non-annealed MoO_3 on top. In both cases, the use of non-annealed MoO_3 improved FF by enhancing R_{SH}. This shows that the electron-blocking ability has been strengthened, whereas both J_{SC} and V_{OC} decreased. This indicates that the energy level mismatching of annealed MoO_x and non-annealed MoO_3 instigates the charge recombination at the interfaces of the active layer, non-annealed MoO_3 layer, and doped SWCNT. The higher PCE of the device D may be attributed to the annealed MoO_3 layer between non-annealed MoO_3 and doped SWCNT functioning as an energy alignment mediator.

When PEDOT:PSS was coated on MoO_x instead of the non-annealed MoO_3, V_{OC} and J_{SC} were enhanced (device E). It is the hydrophilic nature of hydroxyl groups on MoO_x and solution coating method which allow PEDOT:PSS to fill up the pinholes more effectively. Nevertheless, the FF was even lowered, leading to a worse PCE than the device B.

4.1.2. Change in Cathode to LiF/Al

Cathode was changed from Ca/Al to LiF/Al and the performance was drastically increased. The cathode investigation is denoted in Table S4. The device F of Table S3 gave a higher PCE of 1.91% than the device B with 1.47% efficiency. The device G and H fabricated using LiF/Al cathode showed similarly bad result like the device C and D. When PEDOT:PSS is applied along with LiF/Al cathode showed much greater J_{SC} and FF (device I and J). Although the position of the PEDOT:PSS is different, the efficiencies of the device I and J were similar, 2.35% and 2.34%. It is worth remarking that reflecting on many trials, having MoO_x above and below SWCNT improved performance further as the device gave 2.43% efficiency. This is possibly owing to the enhanced doping effect from both sides as there was an infinitesimal reduction in R_S. However, from the UV-IR measurement we could not distinguish the difference because the improvement is subtle. The corresponding *J-V* curves are shown in Figure S8.

Table S3. Photovoltaic performance parameter table for the structural optimization where various layers have been applied.

	Anode	Cathode	V_{OC} (V)	J_{SC} (mAcm^{-2})	FF	R_S (Ωcm^2)	R_{SH} (Ωcm^2)	PCE (%)
A	SWCNT/MoO_3	Ca/Al	0.59	4.74	0.33	1480	2.23E+03	0.92
B	*SWCNT/*MoO_x	Ca/Al	0.61	7.28	0.33	549	9.61E+03	1.47
C	*MoO_x/*SWCNT/MoO_3	Ca/Al	0.51	2.21	0.46	552	1.93E+05	0.52
D	*SWCNT/*MoO_x/MoO_3	Ca/Al	0.50	3.13	0.50	539	2.21E+05	0.74
E	*SWCNT/*MoO_x/PEDOT:PSS	Ca/Al	0.60	5.74	0.30	712	5.73E+04	1.03
F	*SWCNT/*MoO_x	LiF/Al	0.60	7.47	0.43	239	2.05E+04	1.91
G	*MoO_x/*SWCNT/MoO_3	LiF/Al	0.45	0.36	0.38	310	7.82E+04	0.06
H	*SWCNT/*MoO_x/MoO_3	LiF/Al	0.55	3.10	0.42	301	1.46E+04	0.72
I	*MoO_x/*SWCNT/PEDOT:PSS	LiF/Al	0.58	8.44	0.48	163	3.43E+04	2.35
J	*SWCNT/*MoO_x/PEDOT:PSS	LiF/Al	0.59	8.99	0.44	128	1.70E+04	2.34
K	*MoO_x/*SWCNT/*MoO_x/PEDOT:PSS	LiF/Al	0.59	8.84	0.46	116	7.05E+03	2.43

Note: *=Annealed at 300 °C for 3 h under N_2 condition

4.2 *J-V* curves of non annealed and annealed SWCNT OSCs

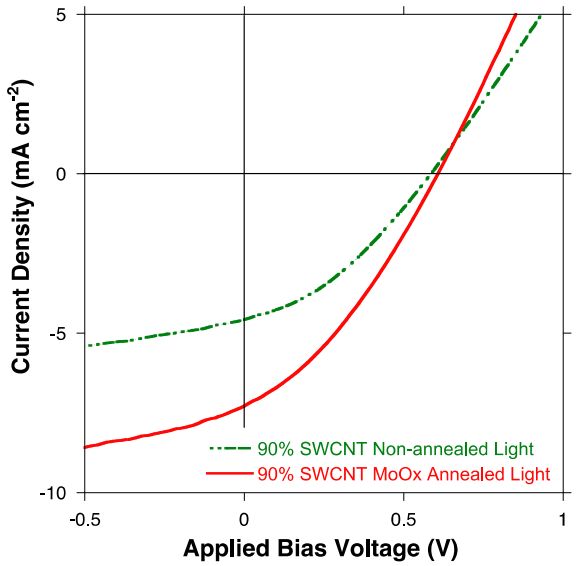

Figure S6. *J-V* curves of the non-annealed device A (dashed green line) and the MoO_x annealed device B (solid red line) under one sun AM1.5G.

4.3 AFM and SEM images of different configurations of electron-blocking layers

The scanning electron microscopy (SEM) images indicate that there are visible pinholes on the MoO_x film (d and e). It reveals that the thermal annealing roughens the morphology as AFM r.m.s. roughness values of 9.7 before annealing and 23.1 after annealing corroborate our observation (a and b). This, according to our studies in Table S2, did not decrease V_{OC} but FF. Thus the MoO_x coverage was fine, but the morphology was the main problem[S5]. Applying PEDOT:PSS smoothened the surface, though it still remained uneven relative to the MoO_3 film (c and f).

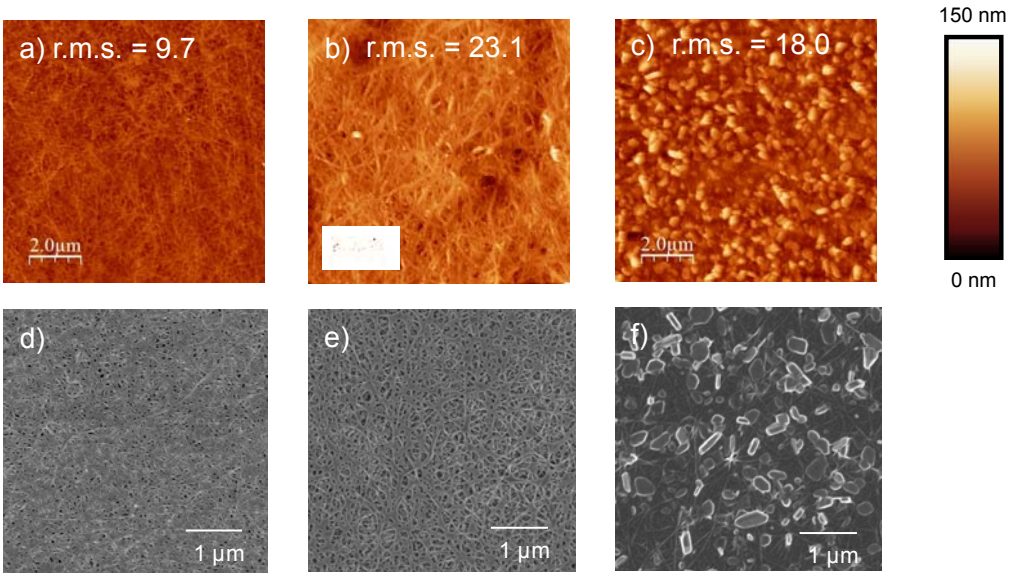

Figure S7. AFM images with r.m.s. roughness values and SEM images of SWCNTs with a) and d) MoO_3 on SWCNT, b) and e) thermally annealed MoO_x on SWCNT, c) and f) PEDOT:PSS soaked thermally annealed MoO_x on SWCNT.

4.4 Effect of various cathodes on SWCNT OSCs

We fabricated different cathodes on a configuration glass/SWCNT/MoO_x annealed. Ohmic type contact formed by cathode affects overall PCE in an OPV device over Schottky type contact, which can bring about diffusion current by accumulating charge carriers[S7]. Hence, rightly tuned cathode can expedite the charge carrier extraction. According to the data, cathodes with low work function like gold must have formed a Schottky contact limiting the charge extraction as V_{OC} and J_{SC} decrease. On the other hand, cathodes like Ca/Al and LiF/Al increased PCEs as their work functions lie far above SWCNT. What is interesting is that despite small difference in work functions between Ca/Al and LiF/Al, LiF/Al showed a much higher performance. This may be ascribed to Ca, which may have caused nonspontaneous electron extraction as Eo and his colleagues have demonstrated[S8]. In addition, although LiF possesses work function of 2.6 eV, it is extremely thin (0.7 nm), so it works as a protective layer and an effective work function can be regarded to be 4.3 eV for LiF/Al which is a different value from 2.9 eV of Ca/Al.

Table S4. Table where various cathodes are applied in a structure SWCNT/MoO_x annealed/P3HT:PCBM/cathode.

Cathode	Work function (-eV)	V_{OC} (V)	J_{SC} (mA/cm^2)	FF	PCE (%)
Ca/Al	2.9	0.61	7.28	0.33	1.47
Al	4.2	0.35	4.55	0.41	0.65
Ag	4.3	0.50	3.97	0.37	0.74
Au	5.3	0.46	1.52	0.49	0.35
LiF/Al	2.6	0.60	7.47	0.43	1.91

Note: The work function values have been taken from the reference S6

4.5 *J-V* curves of the optimized SWCNT OSCs in a P3HT system

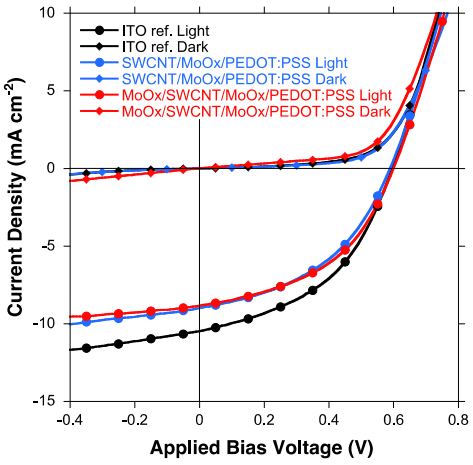

Figure S8. *J-V* curves of the ITO reference device (black lines) and the device J (blue lines) and device K (red lines) under one sun AM1.5G (circle) and dark (diamond) each.

5. Photovoltaic Performance of highly efficient SWCNT OSCs

5.1 Photovoltaic data of SWCNT OSCs and its flexible applications

MoO_x doped SWCNT-based OSC gave the best PCE of 6.04%. Another device in which MoO_3 had not been annealed gave PCE of 5.27%. Considering that there was only PEDOT:PSS's doping effect, the result is still high.

For the flexible applications, both PI and PET were used. Before subjecting to 10-time flexing cycles (radius of curvature: 5 mm), they had given PCEs of 3.78% (PI) and 3.91% (PET). It is a competition between the conductivity and the transmittance as the PI-based OSC has the upper hand in conductivity due to the doping effect from annealed MoO_x, on the other hand PET benefits from the higher transmittance arising from its intrinsic film transparency (Fig. S9). However, our results showed that while J_{SC} of PET-based OSC was higher as expected, R_S was lower. We suspect the shrinking of PI film during MoO_3 thermal annealing process as the PI film technical data sheet reveals 0.14% of its size was shrunk under 200 °C for 30 minutes. Instability of electron-blocking layer was clearly revealed after the 10-time flexing cycles, while the PET-based flexible OSC retained its performance, the PI-based flexible OSC decreased its performance significantly by decreasing R_{SH} and FF.

Table S5. Photovoltaic data of optimized SWCNT OSCs in a PTB7 system and flexible applications on PI and PET.

Device	V_{OC} (V)	J_{SC} (mA/cm^2)	FF	R_S (Ωcm^2)	R_{SH} (Ωcm^2)	PCE (%)
glass/ITO/MoO_3	0.74	15.5	0.64	31.1	1.18E+07	7.31
glass/MoO_x/*SWCNT/*MoO_x/PEDOT:PSS	0.72	13.7	0.61	51.6	1.22E+04	6.04
glass/SWCNT/MoO_3/PEDOT:PSS	0.70	12.7	0.58	94.5	4.00E+04	5.27
PI Film/MoO_x/*SWCNT/*MoO_x/PEDOT:PSS	0.69	11.3	0.44	454	1.15E+05	3.43
After 10-time cyclic flex test on PI flexible OSC	0.70	11.1	0.27	588	3.85E+04	2.10
PET Film/SWCNT/MoO_3/PEDOT:PSS	0.69	12.6	0.45	160	2.06E+03	3.91
After 10-time cyclic flex test on PET flexible OSC	0.69	12.3	0.45	222	2.83E+03	3.82

Note: *=Annealed at 300 °C for 3 h under N_2 condition

5.2 Substrates' optical spectra

The spectra show that PET and glass have higher absorption than PI, especially in the low-wavelengths region. PI's transmittance is almost the same after the thermal annealing which indicates that high temperature on PI does not undermine the substrate's transparency.

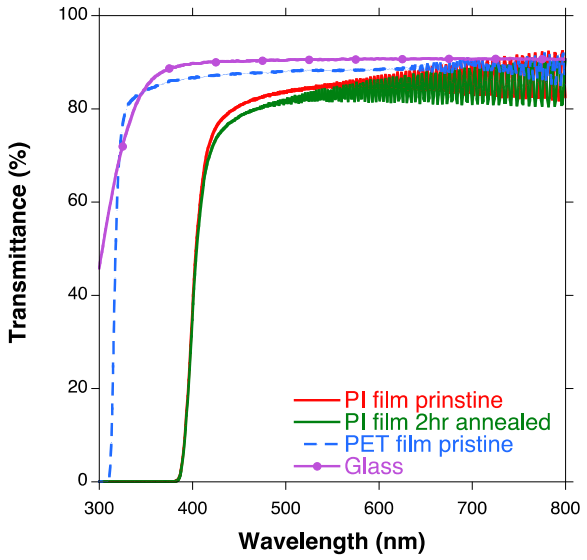

Figure S9. Transmittance data of PI, thermally annealed PI, PET, and bare glass.

5.3 Flexible device performance *J-V* curve

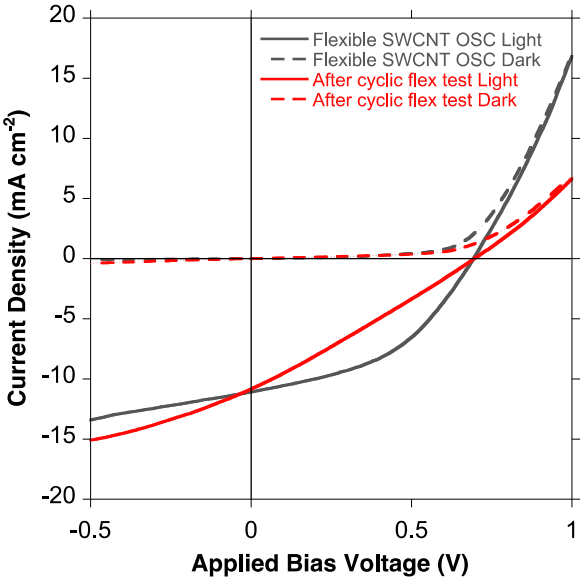

Figure S10 a). *J-V* curves of flexible OSC on PI before and after the cyclic flex test.

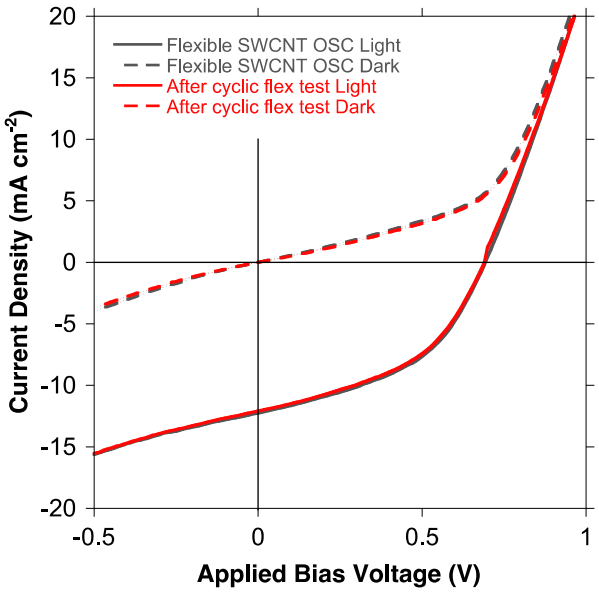

Figure S10 b). *J-V* curves of flexible OSC on PET before and after cyclic flex test.

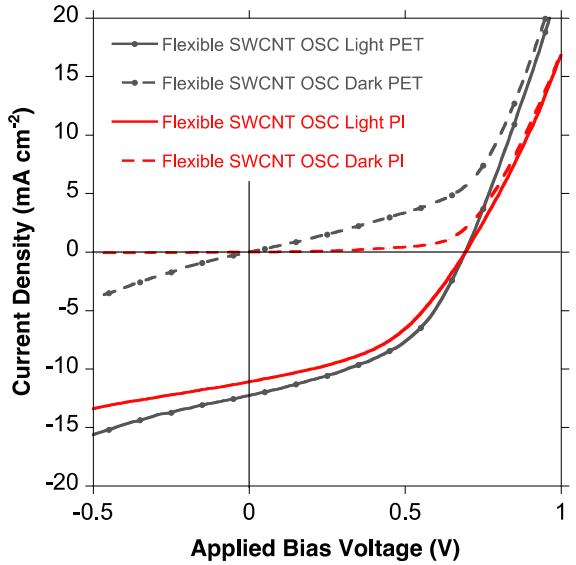

Figure S10 c). *J-V* curve comparison of flexible OSC on both PI and PET.

Supplementary References

[S1] Santo, Y., Jeon, I., Yeo, K. S., Nakagawa, T. & Matsuo, Y. Mixture of [60] and [70] PCBM giving morphological stability in inverted organic solar cells, *Appl. Phys. Lett.* **103**, 073306 (2013).

[S2] Kumar, A., Rosen, N., Devine, R. & Yang, Y. Interface design to improve stability of polymer solar cells for potential space applications. *Energy Environ. Sci.* **4**, 4917-4920 (2011).

[S3] Xu, Z. *et al*. Vertical phase separation in poly(3-hexylthiophene): fullerene derivative blends and its advantage for inverted structure solar cells. *Adv. Funct. Mater.* **19**, 1227–1234 (2009).

[S4] Mestl, G., Ruiz, P., Delmon, B. & Knözinger, H. J. Oxygen-exchange properties of MoO_3: an in situ raman spectroscopy study. *Phys. Chem.* **98**, 11269−11275 (1994).

[S5] Shrotriya, V., Li, G., Yao, Y., Chu, C. W. & Yang, Y. Transition metal oxides as the buffer layer for polymer photovoltaic cells. *Appl. Phys. Lett.* **88**, 073508 (2006).

[S6] Michaelson, H. B. *et al*. The work function of the elements and its periodicity. *J. Appl. Phys.* **48**, 4729−4733 (1977).

[S7] Brabec, C. J. *et al*. Origin of the open circuit voltage of plastic solar cells. *Adv. Funct. Mater.* **11**, 374−380 (2001).

[S8] Eo, Y. S., Rhee, H. W., Chin, B. D. & Yu, J. W. Influence of metal cathode for organic photovoltaic device performance. *Synth. Met.* **159**, 1910−1913 (2009).